Nano Research

ISSN 1998-0124 CN 11-5974/O4
https://doi.org/10.1007/s12274-021-3828-7

Research Article

Triboelectric nanogenerator with mechanical switch and clamp circuit for low ripple output

Xin Yu[1,2], Zhenjie Wang[1,2], Da Zhao[2], Jianwei Ge[1,2], Tinghai Cheng[2,3] (✉), and Zhong Lin Wang[2,3,4] (✉)

[1] School of Electrical and Electronic Engineering, Changchun University of Technology, Jilin 130012, China
[2] Beijing Institute of Nanoenergy and Nanosystems, Chinese Academy of Sciences, Beijing 101400, China
[3] CUSTech Institute of Technology, Zhejiang 325024, China
[4] School of Materials Science and Engineering, Georgia Institute of Technology, Atlanta, GA 30332–0245, USA

Received: 13 July 2021 / **Revised:** 12 August 2021 / **Accepted:** 18 August 2021

ABSTRACT

For new renewable clean energy, triboelectric nanogenerators (TENGs) have shown great potential in response to the world energy crisis. Nevertheless, the alternating-current signal generated by a TENG needs to be converted into a direct-current signal to be effective in applications. Therefore, a power management circuit, comprising a clamp rectifier circuit and a mechanical switch, is proposed for the conversion and produces a signal having a low ripple coefficient. The power management circuit adopts a clamp circuit as the rectifier circuit to increase the rectified voltage, and reduces the loss resulted from the components by reducing the use of discrete components; the electronic switch in the buck regulator circuit is replaced with a mechanical switch to reduce cost and complexity. In a series of experiments, this power management circuit displayed a stable output voltage with a ripple voltage of 0.07 V, crest factor of 1.01, and ripple coefficient of 2.2%. The TENG provides a feasible method to generate stable electric energy and to supply power to low-consumption electronic devices.

KEYWORDS

triboelectric nanogenerator, low ripple coefficient, clamp circuit, mechanical switch, energy harvesting

1 Introduction

In recent years, with the growth in energy demand, various environmental pollution problems caused by fossil energy use are becoming increasingly severe [1–3]. As far as different miniaturized devices are concerned, lithium batteries are conventionally adopted as the preferred source of power [4]. However, their manufacture leaves a large carbon footprint and their cost is not conducive to replace batteries in some particular environments [5]. Therefore, developing renewable clean energy and promoting renewable energy development has become the inevitable option to solve the energy crisis of today. As an effective method to harvest renewable clean energy from the environment, triboelectric nanogenerators (TENGs) have attracted wide attention in the contemporary world [6, 7].

First invented by Wang's group in 2012, the TENG displays many advantages, such as low-cost convenient fabrication and diversity in construction materials [8–11]. A TENG harvests weak energy from various environments, such as wind [12–14], oceans [15], ambient vibrations [16], sound waves [17], raindrops [18], and biomechanical [19] systems. A TENG executes periodic charge transfers between its two electrodes, resulting in an alternating-current (AC) output signal. However, the operation of various miniaturized devices requires a stable direct-current (DC) signal [20, 21]. The electric energy generated by a TENG cannot be effectively applied to a miniaturized device, hence the need for a DC signal processing circuit [22–25]. To convert AC signals into DC signals, a bridge rectifier circuit is commonly adopted [26–29]. The rectified signal has a significant ripple, and thence the pulsating DC signal needs filtering. The standard method is with a step-down regulator circuit [30–32]. The rectifier circuit is combined with a buck regulator circuit to form a power management circuit that is widely used in energy harvesting. However, both these circuits have a number of discrete components, many of which are energy-consuming that create energy losses. This inevitably interferes with the TENG operations and creates an inconvenience to back-end applications.

Herein, to achieve a stable output with a low ripple coefficient, a power management circuit combining a clamp circuit and a mechanical switch is proposed. The circuit includes a rectifier module consisting of a clamp capacitor and a rectifier diode. Leakage current is thereby diminished by reducing the number of rectifier diodes. The clamp capacitor stores the energy of the negative half cycle of the AC signal, which is superimposed with the positive half cycle voltage of the AC signal to improve the voltage output. The buck regulator circuit for the generator includes a mechanical switch, which replaces the electronic switch for on-off operations, thus avoiding the interference caused by current leakage from the electronic switch. This power management circuit provides a more stable electric energy output. Its design achieves a stable output voltage with a ripple voltage of 0.07 V, crest factor of 1.01, and ripple coefficient of 2.2%. This circuit improves the output signal characteristics and generates stable power output enabling the TENG to become a reliable power supply for electronic equipment.

Address correspondence to Tinghai Cheng, chengtinghai@binn.cas.cn; Zhong Lin Wang, zhong.wang@mse.gatech.edu

2 Structure and operation principle

2.1 Structure of power management circuit

In this research, the mechanical-switch-type TENG (MS-TENG) consists of a supporting component, a power generation unit, a rotating shaft, a mechanical switch, and a conductive slip ring connected to the switch (see Fig. 1(a)). Figures 1(b)–1(e) show separately these various components of the MS-TENG. The mechanical switch comprises a stator, which is composed of polylactic acid (PLA), acrylic sheet with copper strips attached, and a rotor which is composed of PLA with a copper strip attached. The rotor contains two symmetrical structures; one at the end of the rotor that combines with the stator to form switch S_1, and the other a terminal which combines with the stator to form switch S_2. Switch S_1 is inserted in the buck regulator circuit, whereas switch S_2 is used instead of diode D_2 to suppress charge backflow and verifies the restraining backflow functioning of diode D_2 (Fig. S1 in the Electronic Supplementary Material (ESM)).

In the operation process of the mechanical switch (Fig. 2(a)), the mechanical switch S_1 is used to instead of a common electronic switch in the buck regulator circuit. The switch on the rotating shaft is connected to an external wire through the conductive slip ring, and the copper strips on the acrylic sheet are connected to another external wire. These two wires act as connectors of the switch. The rotating shaft drives the switch to rotate clockwise. When the copper strip attached to the switch comes into physical contact with the copper strips on the acrylic sheet, the switch is turned on. As the switch continues to rotate, the copper strips are no longer in contact, and thus the switch disconnects the circuit.

The power management circuit (Fig. 2(b)) consists of a rectifier

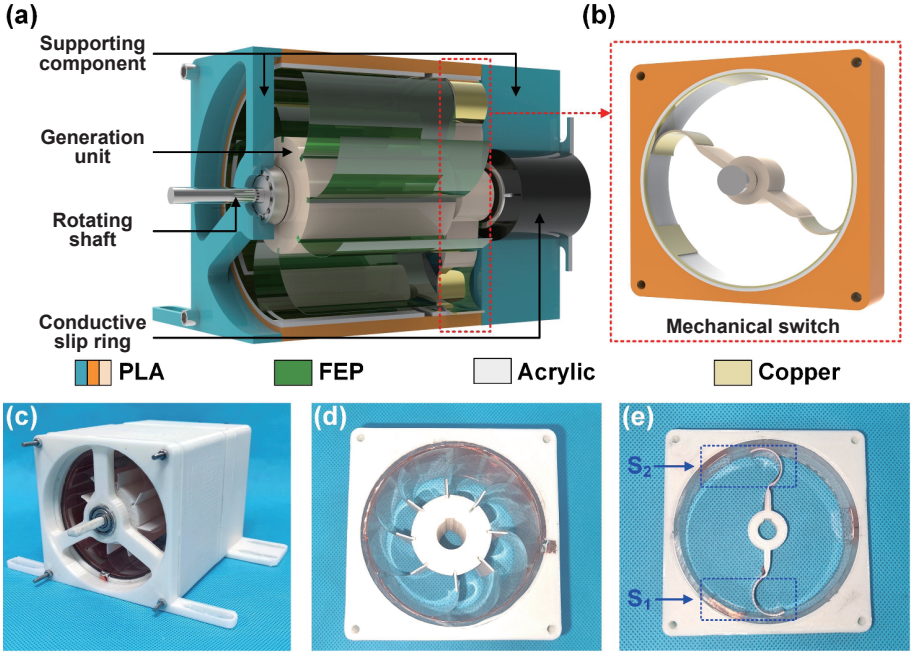

Figure 1 Mechanical-switch-type triboelectric nanogenerator (MS-TENG). (a) and (b) Schematic diagram of the overall structure. Photographs of (c) MS-TENG, (d) generation unit, (e) mechanical switch.

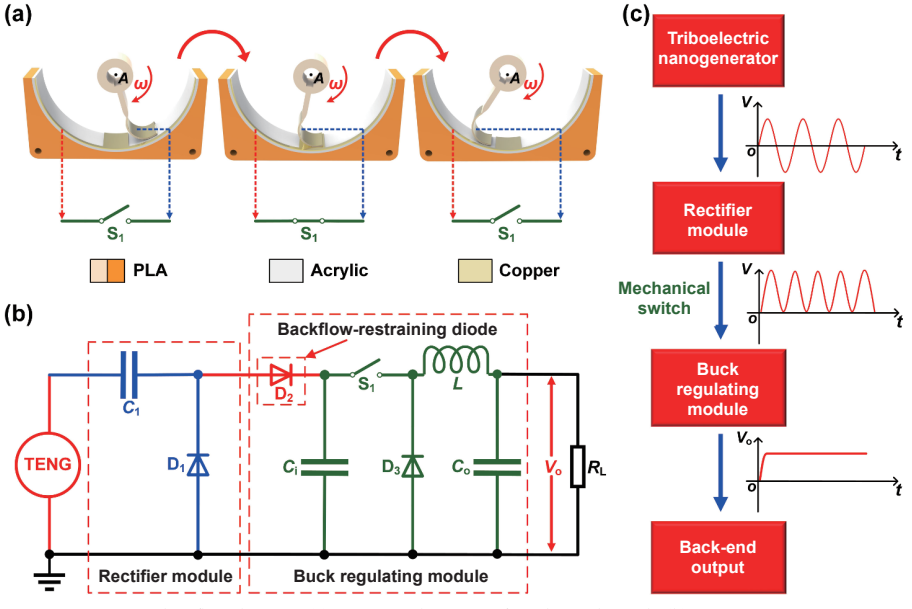

Figure 2 The power management circuit and its flow diagram: (a) operational process of mechanical switch, (b) power management circuit, and (c) flow diagram of a power management circuit.

module and a buck regulator module. The rectifier module consists of a clamp capacitor and a rectifier diode. The buck regulator module consists of two capacitors, two diodes, an inductor, and a switch. Power management (Fig. 2(c)) begins with an AC signal generated by the TENG which is changed into a pulsating DC signal by the rectifier module, which has a significant ripple and needs to be processed by the buck regulator module to stabilize the output. The buck regulator module uses a typical buck regulator circuit, which includes inductor L and output capacitor C_o to form a low-pass filter to pass the input DC component and suppress the harmonic input component. When the circuit operates in a steady-state, the voltage V_o across the load resistor R_L has a significant DC component with only a tiny ripple.

2.2 Operation principle of circuit

A clamp circuit is used as a rectifier module (Fig. 3(a)), consisting typically of a rectifier diode and a clamp capacitor. When the current flows into the TENG in a counterclockwise direction (Fig. 3(b)), the branch circuit of the clamp diode D_1 is equivalent to a short circuit and current flows through it because of the forward conduction characteristics of the diode. Concurrently, the load is clamped, and the TENG charges clamp capacitor C_1. When the current flows out of the TENG in the clockwise direction (Fig. 3(c)), the clamp diode branch circuit is equivalent to an open circuit and, with the reverse turn-off characteristic of the diode, the current flows only through load R_L. The voltage at both ends of the load is generated by a superposition of the voltage across the clamp capacitor and the voltage across the generation unit.

The difference between our buck regulator module (Fig. 3(d)) and a standard buck regulator circuit is that a mechanical switch S_1 is used to control the on-off operation of the circuit. At the same time, a backflow-restraining diode D_2 is added to prevent charge on the input capacitor C_i from flowing back to the rectifier module. The initial voltage across the load is 0 V (Fig. 3(e)). When switch S_1 is in the off state, the input capacitor filters the pulsating DC signal generated by the rectifier module for the first time. When switch S_1 is in the on-state (Fig. 3(f)), the branch circuit with the freewheeling diode D_3 is equivalent to an open circuit. The filtered primary signal passes through the low-pass filter composed of the output capacitor C_o and inductor L. Meanwhile, the output capacitor is being charged, and its voltage rises. When switch S_1 is turned off again, the input voltage U_i discharges across the input capacitor, and the back-end circuit forms a loop through the freewheeling diode. When the switch is turned on, the inductor current increases and stores energy in the inductor; when the switch is turned off, the inductor current decreases thereby releasing energy. By this fluctuation, a ripple current generated by the inductor flows to the output capacitor to generate a ripple voltage. When charging of the output capacitor is faster than discharging over one cycle, the capacitor voltage increases, which slows charging and quickens discharging in the following cycle. The rate of increase in capacitor voltage slows down. When charging is slower than discharging, the capacitor voltage decreases, and charging diminishes. Discharging increases in the following cycle, and the rate of decrease of the capacitor voltage slows, thereby achieving finally a charge-discharge balance.

3 Results and discussion

3.1 Rectification circuit test

The clamp rectifier circuit (Fig. 4(a)) and the conventional bridge rectifier circuit (Fig. 4(b)) were both tested. In a comparison, the clamp circuit requires few discrete components, and for the same load, circuit losses are low. The clamp circuit uses 4.7 nF polypropylene capacitor (also called CBB capacitor) with a withstand voltage of 2,000 V, the voltage superimposed by the clamp capacitor and the TENG improve the load voltage output. To analyze more intuitively the differences between the two rectifier circuits, specific comparisons were made (Table S1 in the ESM). Time variations of the output voltage under load resistances

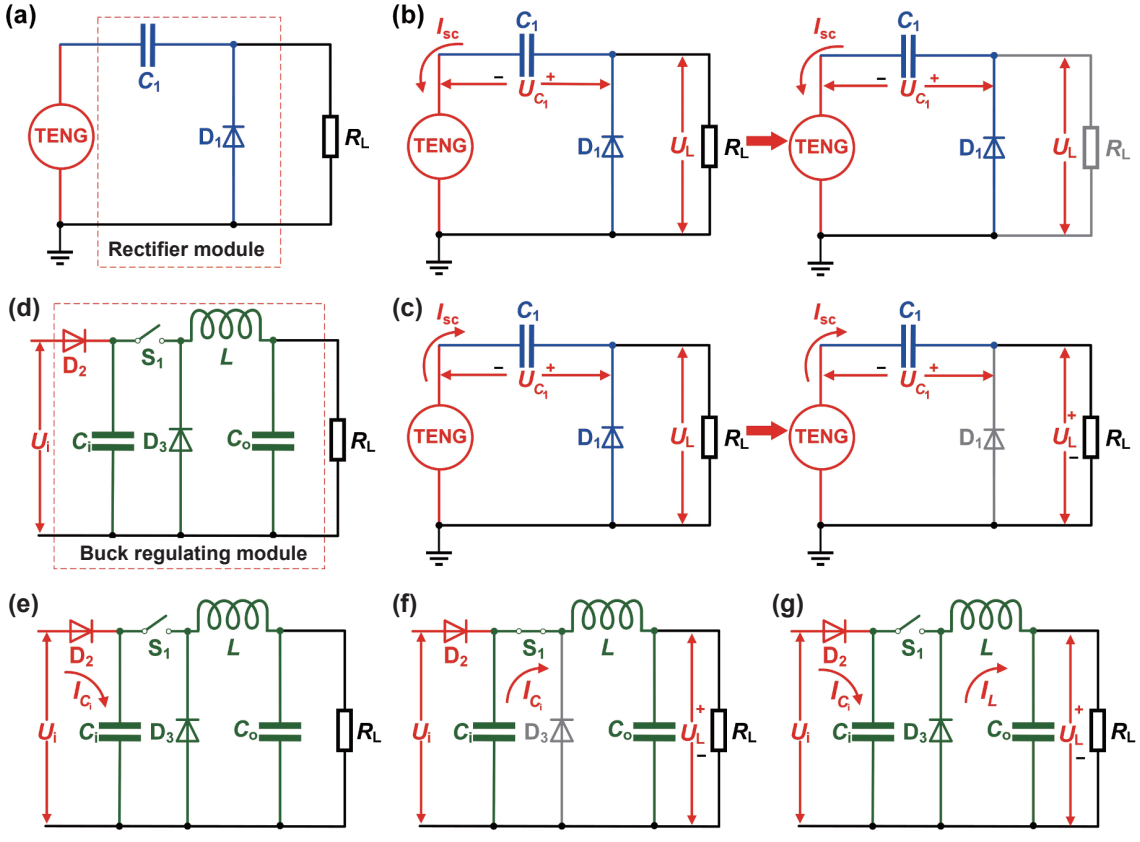

Figure 3 Power management circuit: (a) rectifier module and (b) and (c) its operating principle, and (d) buck regulating module and (e)–(g) its operating principle.

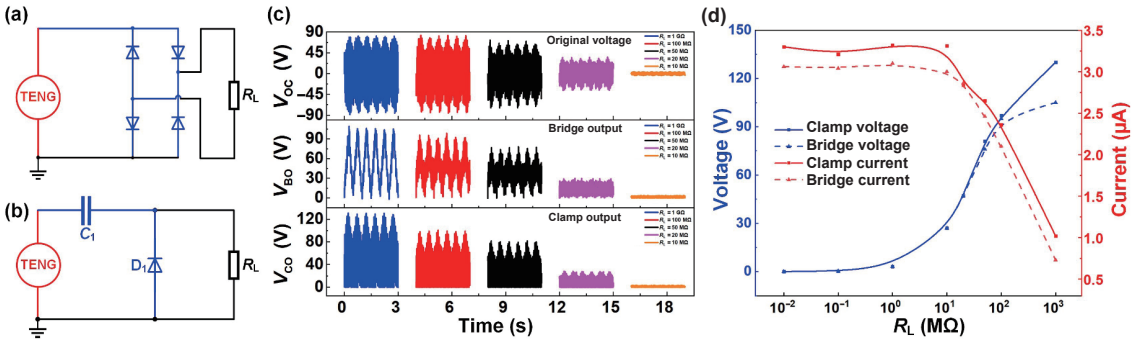

Figure 4 Comparison of two rectifier circuits: (a) and (b) circuit diagrams, (c) comparison of output after and before rectification, and (d) output characteristic curves of the two circuits under various loads.

of 10 MΩ, 20 MΩ, 50 MΩ, 100 MΩ, and 1 GΩ were recorded (Fig. 4(c)); here, V_{OC} denotes the original voltage without the rectifier module, V_{BO} the output voltage across the load after bridge rectification, and V_{CO} the output voltage across the load after clamp rectification. In addition, the voltage and current curves (Fig. 4(d)) of the bridge rectifier (dashed lines) and clamp rectifier (solid lines) were measured under different loads. In a comparison, under identical loading, the latter has higher output characteristics.

3.2 Voltage regulator circuit test

The AC signal generated by TENG is converted into a pulsating DC signal after passing through the rectifier circuit, but often has a significant ripple voltage and hence cannot be applied in subsequent steps. A typical processing method is to connect a filter capacitor C_o in parallel across the load. With our resistance-capacitance (RC) voltage regulator circuit (Fig. 5(a)), the AC component in the pulsating DC signal rectified by the clamp circuit flows to ground through the capacitor because it restrains and stores the DC component. Similarly, the backflow-restraining diode D_2 added after the clamp circuit prevents any discharging back towards the clamp circuit. The output voltage for three load resistances R_L (1, 10, and 100 MΩ) were recorded (Figs. 5(b)–5(d)). In addition, for fixed output capacitance of 0.1 μF, the output voltage during charging were recorded for various load resistances (Fig. 5(e)). With increasing filter capacitor C_o, the voltage rise time increases, and the value of the output voltage V_o is determined by the load resistance R_L. From Fig. 5(f), when the load resistance is fixed at 1 MΩ, the output capacitance C_o rises from 0.1 to 100 μF, and the voltage rise time increases with increasing capacitance. The output voltage remains unchanged. Furthermore, with fixed output capacitor C_o of 10 μF, the voltage rise time and the output voltage increase with increasing load (Fig. 5(g)). The voltage rise time is determined from the resistance and the capacitance; with the rise in both, the time taken for V_o to reach a steady-state increases. Because the impedance between the load resistor and the TENG must match, the steady value of the output voltage V_o is related to the load resistance but is independent of the capacitance.

3.3 Power management circuit test

An alternative method to deal with pulsating DC power signals is to use a buck regulator circuit to step down and stabilize the rectified output. Compared with a RC voltage regulator circuit, this circuit adds a switch S_1, an inductor L, an input capacitor C_i, and a freewheeling diode D_2. The input capacitor performs a primary filtering on the pulsating DC signal. With on-to-off switching, the energy in the input capacitor is transmitted to the back-end circuit. In this paper, the input capacitor uses the same CBB capacitor as the clamp capacitor, and the output capacitor uses an electrolytic capacitor with polarity.

The change in the output voltage (Figs. 6(a)–6(c)) was recorded for a load of 10 MΩ, an output capacitance of 1 μF, and input capacitances of 1, 10, and 100 nF (Figs. 6(a)–6(c), respectively). With capacitive reactance matching between the MS-TENG and the input capacitor, the voltage V_i on the input capacitor C_i increases accordingly as the input capacitor approaches the internal capacitive reactance of the MS-TENG. Figures 6(d)–6(f) show the influence of a varying inductance on the output voltage and voltage rise time when input capacitance is 1 nF, the output

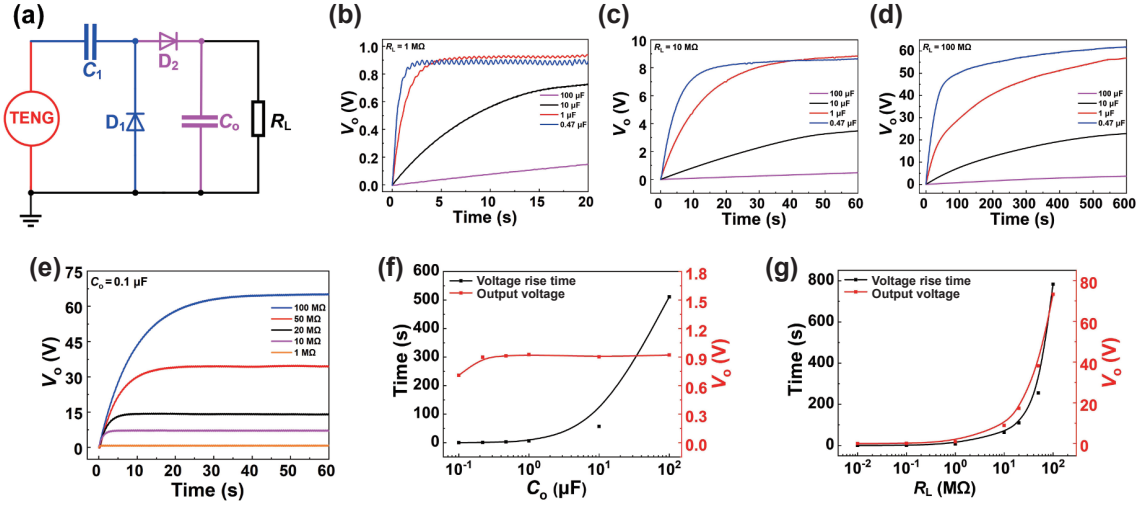

Figure 5 Charging characteristics for the RC voltage regulator circuit: (a) circuit model, (b)–(d) output voltage variation curves obtained for three output capacitances, (e) output voltage curves for five different loads and fixed output capacitance, and (f) and (g) curves of the voltage rise time and output voltage variation obtained by varying the output capacitance and load resistance, respectively.

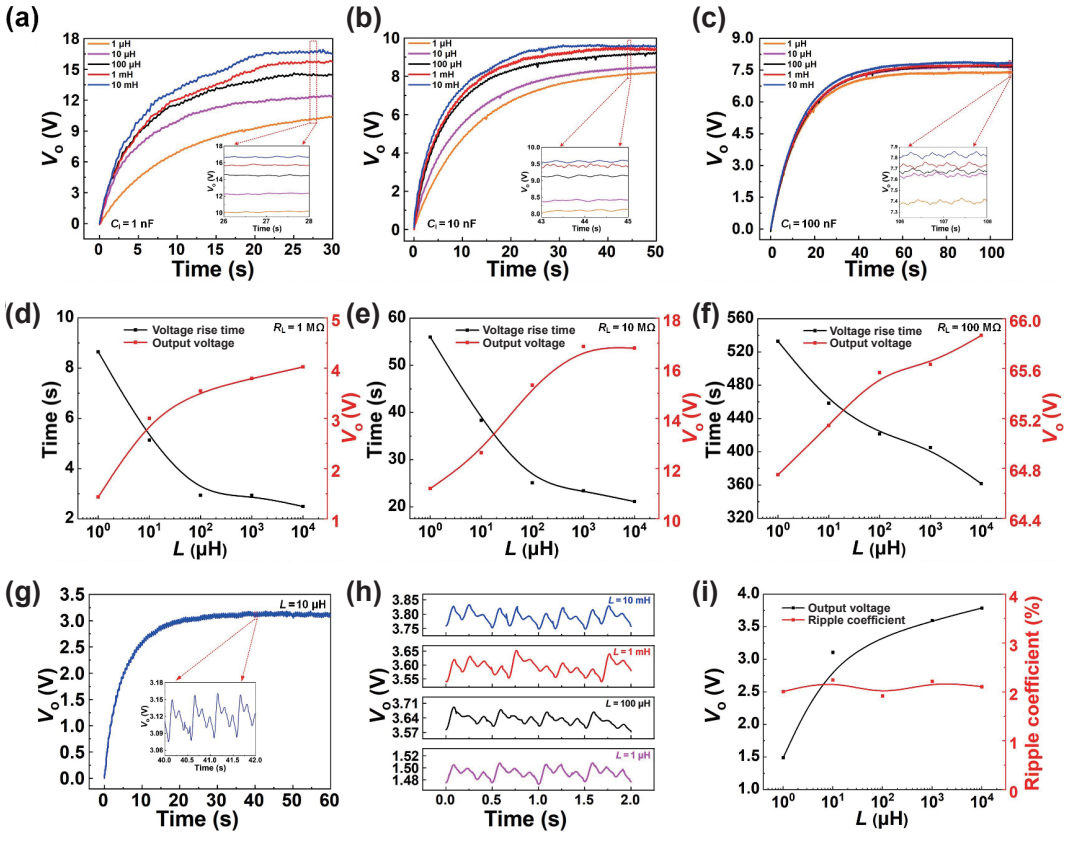

Figure 6 Testing the mechanical-switch-type TENG: (a)–(c) output voltage variation of the voltage rise time and output voltage for various input capacitances and different loads without a backflow-restraining diode, (d)–(f) influence of varying the inductance on voltage rise time and output voltage under different loads, and (g)–(i) output characteristics for a fixed load resistance of 1 MΩ, and an output capacitance of 10 μF.

capacitance is 1 μF, and the load resistance is 1, 10, and 100 MΩ (Figs. 6(d)–6(f), respectively). With increasing inductance, the voltage rise time decreases and the output voltage rises. During on-off switching of the inductor, energy storage and discharge alternate repeatedly. Inductors store electric energy within the magnetic field of the circuit. The larger the inductance is, the larger the stored and released electric energy will be. The voltage rise time is also shortened accordingly. When an AC signal flows through the inductor, time varying magnetic lines of force appear around the inductor. These lines of force generate an induced electromotive force at both ends of the coil, equivalent to a new power supply. With increasing inductance, the induced electromotive force increases, and accordingly, the output voltage also increases.

Figure 6(g) shows the time variation of the output voltage for the MS-TENG with a fixed load of 1 MΩ, an input capacitance of 1 nF, and an output capacitance of 10 μF. The time dependence of the output voltage for various inductances is given in Fig. 6(h), and the variation of output voltage and ripple coefficient with inductance is given in Fig. 6(i). The experimental tests show that the ripple voltage is 0.07 V, the crest factor is 1.01, and the ripple coefficient is 2.2%. The voltage rises with increasing inductance, whereas the ripple coefficient is stable at approximately 2%. The ripple voltage, crest factor, and ripple coefficient reflect the stability of the output voltage; the lower these values are, the more stable the output is. The specific method of calculation is explained in the ESM.

4 Conclusions

In summary, a power management circuit designed by combining clamp rectifier circuit and mechanical switch is proposed, which can convert AC signal generated by TENG into DC signal with low ripple coefficient. The clamp rectifier circuit comprises a clamp capacitor and a rectifier diode, which can improve the power transmission efficiency by reducing discrete components, at the same time, the output voltage is increased by the clamping effect of the diode. The buck regulating circuit based on mechanical switch filters the pulsating DC signal generated by the rectifier unit into a stable DC signal with a low ripple and finally outputs a stable voltage with a ripple voltage of 0.07 V, crest factor of 1.01, and ripple coefficient of 2.2%. This circuit can resolve significant ripple and high crests in the output voltage of conventional power management circuit. This research has demonstrated a feasible approach for a TENG device to harvest renewable clean energy from the environment and convert it into a stable electric energy signal that can readily power electronic equipment.

5 Experimental section

5.1 Fabrication of the MS-TENG

The MS-TENG has dimensions of 140 mm (length) × 100 mm (width) × 100 mm (height). The supporting component, power generation unit, rotating shaft, and mechanical switch are all made by three-dimensional (3D) printing, and the printing material is PLA. The flexible membrane (thickness 100 μm, width 60 mm) uses fluorinated ethylene propylene (FEP). Sixteen copper electrodes (thickness 100 μm, width 15 mm, length 60 mm) are evenly distributed on the power generation unit.

5.2 Electrical measurement

Rotating mechanical energy output by a two-phase hybrid stepping motor (57BYGH56D8EIS-P, Aokong, China) is used to power MS-TENG. The output signal of the generator is harvested by an electrometer (6514, Keithley, USA). The display and storage

of data are performed by installing the software LabVIEW with the computer.

Acknowledgements

The authors are grateful for the supports received from the Scientific Research Project of Education Department of Jilin Province (No. JJKH20210736KJ), the National Key R&D Project from the Minister of Science and Technology (Nos. 2016YFA0202701 and 2016YFA0202704), and the Beijing Municipal Science and Technology Commission (No. Z171100002017017).

Conflict of interest

The authors declare no conflict of interest.

Electronic Supplementary Material: Supplementary material (additional figures and movies, including verification of backflow suppression diode, comparison table of two kinds of rectifier circuit parameters and demonstration video of power management circuit) is available in the online version of this article at https://doi.org/10.1007/s12274-021-3828-7.

References

[1] Wang, Z. L. Entropy theory of distributed energy for internet of things. *Nano Energy* **2019**, *58*, 669–672.

[2] Jiang, T.; Pang, H.; An, J.; Lu, P. J.; Feng, Y. W.; Liang, X.; Zhong, W.; Wang, Z. L. Robust swing-structured triboelectric nanogenerator for efficient blue energy harvesting. *Adv. Energy Mater.* **2020**, *10*, 2000064.

[3] Wang, Z. L.; Wu, W. Z. Nanotechnology-enabled energy harvesting for self-powered micro-/nanosystems. *Angew. Chem., Int. Ed.* **2012**, *51*, 11700–11721.

[4] Moreno-Brieva, F.; Merino, C. African international trade in the global value chain of lithium batteries. *Mitig. Adapt. Strat. Glob. Change* **2020**, *25*, 1031–1052.

[5] Cheng, T. H.; Gao, Q.; Wang, Z. L. The current development and future outlook of triboelectric nanogenerators: A Survey of literature. *Adv. Mater. Technol.* **2019**, *4*, 1800588.

[6] Ahmed, A.; Hassan, I.; Ibn-Mohammed, T.; Mostafa, H.; Reaney, I. M.; Koh, L. S. C.; Zu, J.; Wang, Z. L. Environmental life cycle assessment and techno-economic analysis of triboelectric nanogenerators. *Energy Environ. Sci.* **2017**, *10*, 653–671.

[7] Wang, Z. L. Triboelectric nanogenerator (TENG)-sparking an energy and sensor revolution. *Adv. Energy Mater.* **2020**, *10*, 2000137.

[8] Wang, Z. L. Triboelectric nanogenerators as new energy technology for self-powered systems and as active mechanical and chemical sensors. *ACS Nano* **2013**, *7*, 9533–9557.

[9] Zou, H. Y.; Zhang, Y.; Guo, L. T.; Wang, P. H.; He, X.; Dai, G. Z.; Zheng, H. W.; Chen, C. Y.; Wang, A. C.; Xu, C. et al. Quantifying the triboelectric series. *Nat. Commun.* **2019**, *10*, 1427.

[10] Wang, Z. L.; Zhu, G.; Yang, Y.; Wang, S. H.; Pan, C. F. Progress in nanogenerators for portable electronics. *Mater. Today* **2012**, *15*, 532–543.

[11] Liu, W. L.; Wang, Z.; Hu, C. G. Advanced designs for output improvement of triboelectric nanogenerator system. *Mater. Today* **2021**, *45*, 93–119.

[12] Han, K.; Luo, J. J.; Feng, Y. W.; Lai, Q. S.; Bai, Y.; Tang, W.; Wang, Z. L. Wind-driven radial-engine-shaped triboelectric nanogenerators for self-powered absorption and degradation of NO_x. *ACS Nano* **2020**, *14*, 2751–2759.

[13] Hu, J.; Pu, X. J.; Yang, H. M.; Zeng, Q. X.; Tang, Q.; Zhang, D. Z.; Hu, C. G.; Xi, Y. A flutter-effect-based triboelectric nanogenerator for breeze energy collection from arbitrary directions and self-powered wind speed sensor. *Nano Res.* **2019**, *12*, 3018–3023.

[14] Zhong, Y. M.; Zhao, H. B.; Guo, Y. C.; Rui, P. S.; Shi, S. W.; Zhang, W.; Liao, Y. L.; Wang, P. H.; Wang, Z. L. An easily assembled electromagnetic-triboelectric hybrid nanogenerator driven by magnetic coupling for fluid energy harvesting and self-powered flow monitoring in a smart home/city. *Adv. Mater. Technol.* **2019**, *4*, 1900741.

[15] Yin, M. F.; Yu, Y.; Wang, Y. Q.; Wang, Z.; Lu, X. H.; Cheng, T. H.; Wang, Z. L. Multi-plate structured triboelectric nanogenerator based on cycloidal displacement for harvesting hydroenergy. *Extreme Mech. Lett.* **2019**, *33*, 100576.

[16] Quan, T.; Yang, Y. Fully enclosed hybrid electromagnetic-triboelectric nanogenerator to scavenge vibrational energy. *Nano Res.* **2016**, *9*, 2226–2233.

[17] Zhao, H. F.; Xiao, X.; Xu, P.; Zhao, T. C.; Song, L. G.; Pan, X. X.; Mi, J. C.; Xu, M. Y.; Wang, Z. L. Dual-tube helmholtz resonator-based triboelectric nanogenerator for highly efficient harvesting of acoustic energy. *Adv. Energy Mater.* **2019**, *9*, 1902824.

[18] Jošt, M.; Lipovšek, B.; Glažar, B.; Al-Ashouri, A.; Brecl, K.; Matič, G.; Magomedov, A.; Getautis, V.; Topič, M.; Albrecht, S. Perovskite solar cells go outdoors: Field testing and temperature effects on energy yield. *Adv. Energy Mater.* **2020**, *10*, 2000454.

[19] Lu, X. H.; Xu, Y. H.; Qiao, G. D.; Gao, Q.; Zhang, X. S.; Cheng, T. H.; Wang, Z. L. Triboelectric nanogenerator for entire stroke energy harvesting with bidirectional gear transmission. *Nano Energy* **2020**, *72*, 104726.

[20] Ding, W. B.; Zhou, J. F.; Cheng, J.; Wang, Z. Z.; Guo, H. Y.; Wu, C. S.; Xu, S. X.; Wu, Z. Y.; Xie, X.; Wang, Z. L. TriboPump: A low-cost, hand-powered water disinfection system. *Adv. Energy Mater.* **2019**, *9*, 1901320.

[21] Du, X. Y.; Li, N. W.; Liu, Y. B.; Wang, J. N.; Yuan, Z. Q.; Yin, Y. Y.; Cao, R.; Zhao, S. Y.; Wang, B.; Wang, Z. L. et al. Ultra-robust triboelectric nanogenerator for harvesting rotary mechanical energy. *Nano Res.* **2018**, *11*, 2862–2871.

[22] Graham, S. A.; Chandrarathna, S. C.; Patnam, H.; Manchi, P.; Lee, J. W.; Yu, J. S. Harsh environment-tolerant and robust triboelectric nanogenerators for mechanical-energy harvesting, sensing, and energy storage in a smart home. *Nano Energy* **2021**, *80*, 105547.

[23] Kim, D.; Jin, I. K.; Choi, Y. K. Ferromagnetic nanoparticle-embedded hybrid nanogenerator for harvesting omnidirectional vibration energy. *Nanoscale* **2018**, *10*, 12276–12283.

[24] Li, N. W.; Yin, Y. Y.; Du, X. Y.; Zhang, X. L.; Yuan, Z. Q.; Niu, H. D.; Cao, R.; Fan, W.; Zhang, Y.; Xu, W. H. et al. Triboelectric nanogenerator-enabled dendrite-free lithium metal batteries. *ACS Appl. Mater. Interfaces* **2019**, *11*, 802–810.

[25] Niu, S. M.; Zhou, Y. S.; Wang, S. H.; Liu, Y.; Lin, L.; Bando, Y.; Wang, Z. L. Simulation method for optimizing the performance of an integrated triboelectric nanogenerator energy harvesting system. *Nano Energy* **2014**, *8*, 150–156.

[26] Ouyang, Q. L.; Feng, X. L.; Kuang, S. Y.; Panwar, N.; Song, P. Y.; Yang, C. B.; Yang, G.; Hemu, X.; Zhang, G.; Yoon, H. S. et al. Self-powered, on-demand transdermal drug delivery system driven by triboelectric nanogenerator. *Nano Energy* **2019**, *62*, 610–619.

[27] Qin, H. F.; Gu, G. Q.; Shang, W. Y.; Luo, H. C.; Zhang, W. H.; Cui, P.; Zhang, B.; Guo, J. M.; Cheng, G.; Du, Z. L. A universal and passive power management circuit with high efficiency for pulsed triboelectric nanogenerator. *Nano Energy* **2020**, *68*, 104372.

[28] Ren, Z. Y.; Zheng, Q.; Wang, H. B.; Guo, H.; Miao, L. M.; Wan, J.; Xu, C.; Cheng, S. Y.; Zhang, H. X. Wearable and self-cleaning hybrid energy harvesting system based on micro/nanostructured haze film. *Nano Energy* **2020**, *67*, 104243.

[29] Wang, F.; Tian, J. W.; Ding, Y. F.; Shi, Y. X.; Tao, X. L.; Wang, X. L.; Yang, Y.; Chen, X. Y.; Wang, Z. L. A universal managing circuit with stabilized voltage for maintaining safe operation of self-powered electronics system. *iScience* **2021**, *24*, 102502.

[30] Xi, F. B.; Pang, Y. K.; Li, W.; Jiang, T.; Zhang, L. M.; Guo, T.; Liu, G. X.; Zhang, C.; Wang, Z. L. Universal power management strategy for triboelectric nanogenerator. *Nano Energy* **2017**, *37*, 168–176.

[31] Xi, F. B.; Pang, Y. K.; Liu, G. X.; Wang, S. W.; Li, W.; Zhang, C.; Wang, Z. L. Self-powered intelligent buoy system by water wave energy for sustainable and autonomous wireless sensing and data transmission. *Nano Energy* **2019**, *61*, 1–9.

[32] Xia, K. Q.; Zhu, Z. Y.; Fu, J. M.; Li, Y. M.; Chi, Y.; Zhang, H. Z.; Du, C. L.; Xu, Z. W. A triboelectric nanogenerator based on waste tea leaves and packaging bags for powering electronic office supplies and behavior monitoring. *Nano Energy* **2019**, *60*, 61–71.